BJ www.biochemj.org

BJ Cell

Biochem. J. (2009) **422**, 383–392 (Printed in Great Britain) doi:10.1042/BJ20090010

online data

Specific inhibition of tissue kallikrein 1 with a human monoclonal antibody reveals a potential role in airway diseases

Daniel J. SEXTON*[1], Ting CHEN*, Diana MARTIK*, Petr KUZMIC†, Guannan KUANG*, Jie CHEN*, Andrew E. NIXON*, Bruce L. ZURAW‡, Rosanna M. FORTEZA§, William M. ABRAHAM¶ and Clive R. WOOD*

*Discovery Research, Dyax Corp., 300 Technology Square, Cambridge, MA 02139, U.S.A., †BioKin Ltd, 15 Main Street, Suite 232, Watertown, MA 02472, U.S.A., ‡Department of Medicine, University of California San Diego, 9500 Gilman Dr., La Jolla, CA 92093, U.S.A., §Division of Pulmonary and Critical Care Medicine, University of Miami, Miller School of Medicine, Miami, FL 33136, U.S.A., and ¶Department of Research, Mount Sinai Medical Center, 4300 Alton Road, Miami Beach, FL 33140, U.S.A.

KLK1 (tissue kallikrein 1) is a member of the tissue kallikrein family of serine proteases and is the primary kinin-generating enzyme in human airways. DX-2300 is a fully human antibody that inhibits KLK1 via a competitive inhibition mechanism ($K_i = 0.13$ nM). No binding of DX-2300 to KLK1 was observed in a surface-plasmon-resonance biosensor assay when KLK1 was complexed to known active-site inhibitors, suggesting that DX-2300 recognizes the KLK1 active site. DX-2300 did not inhibit any of the 21 serine proteases that were each tested at a concentration of 1 μM. We validated the use of DX-2300 for specific KLK1 inhibition by measuring the inhibition of KLK1-like activity in human urine, saliva and bronchoalveolar lavage fluid, which are known to contain active KLK1. In human tracheobronchial epithelial cells grown at the air/liquid interface, DX-2300 blocked oxidative-stress-induced epidermal-growth-factor receptor activation and downstream mucus cell proliferation and hypersecretion, which have been previously shown to be mediated by KLK1. In an allergic sheep model of asthma, DX-2300 inhibited both allergen-induced late-phase bronchoconstriction and airway hyper-responsiveness to carbachol. These studies demonstrate that DX-2300 is a potent and specific inhibitor of KLK1 that is efficacious in *in vitro* and *in vivo* models of airway disease.

Key words: antibody inhibition of protease, asthma, bradykinin, chronic obstructive pulmonary disease, kallikrein, kinin.

INTRODUCTION

KLK1 (tissue kallikrein 1) is a member of the tissue kallikrein family of serine proteases, which, in humans, comprises 15 proteases and constitutes the largest contiguous cluster of any family of proteases on the human genome [1,2]. KLK1 has been referred to as 'true tissue kallikrein', because it was the first kallikrein to be described and it appears to be the only tissue kallikrein family member with significant kininogenase (i.e. kinin-generating) activity [1]. Kinins are potent bioactive peptides that trigger vasodilation, vascular leakage, pain, smooth-muscle contraction and the secretion of pro-inflammatory mediators [3–6]. Kinins act through two G-protein-coupled receptors: the constitutively and widely expressed B2 receptor and the inducible B1 receptor [5]. Expression of the B1 receptor is induced by cytokines, growth factors and other stimuli, such as lipopolysaccharides, associated with the onset of chronic inflammation [5]. The kallikrein–kinin system has been implicated in numerous models of diseases, including inflammation, cancer and pathologies related to cardiovascular, renal and central nervous systems [7–9].

KLK1 cleaves both low-molecular-mass kininogen and HMMK (high-molecular-mass kininogen) at two sites to release the decapeptide kinin Lys-bradykinin (Lys-Arg-Pro-Pro-Gly-Phe-Ser-Pro-Phe-Arg), whereas KLKb1 (plasma kallikrein) generates the nonapeptide kinin bradykinin, but only from HMMK [10]. Plasma kallikrein is a serine protease with kininogenase activity, but it is not a member of the tissue kallikrein family. Plasma kallikrein is primarily expressed by the liver and circulates as a zymogen, known as prekallikrein [10], whereas KLK1 is secreted in response to various stimuli from cells such as neutrophils and macrophages as well as from tissues such as intestine, kidney, pancreas, salivary glands and tracheobronchial submucosal glands [11–15].

In the airways, kinins have been shown to mediate bronchoconstriction, increase vascular permeability and induce mucus hypersecretion, as well as trigger cholinergic and sensory nerve stimulation [16–18]. One of the key observations implicating kinins in airway diseases was the discovery that bradykinin inhalation causes immediate bronchonconstriction in asthmatic patients, but not in normal volunteers [16]. Similarly, bradykinin inhalation by animal models of asthma also induces bronchoconstriction [19]. The effects of kinins in the airways appear to be primarily mediated by the B2 G-protein-coupled receptor, since B2 receptor antagonists have shown efficacy in various animal models of asthma [19,20]. Furthermore, a B2 receptor antagonist improved lung function in patients with asthma in a manner consistent with an anti-inflammatory mechanism of action [21]. However, B1 receptor antagonists have also been effective in reducing lung inflammation in rodent models of asthma [20]. The observation that both bradykinin receptors may be involved in allergen-induced responses in the lung suggests that blocking kinin generation with a specific inhibitor of the primary airway kininogenase

Abbreviations used: AEBSF, 4-(2-aminoethyl)benzenesulfonyl fluoride hydrochloride; AHR, airway hyper-responsiveness; AIC_c, Akaike Information Criterion; ALI, air/liquid interface; AMC, 7-amido-4-methylcoumarin; AUC, area under the curve; BAL, bronchoalveolar lavage; BU, breath units; EAR, early-phase airway response; EGF, epidermal growth factor; EGFR, EGF receptor; HBE, human tracheobronchial epithelial cells; HMMK, high-molecular-mass kininogen; KLK1, tissue kallikrein 1; LAR, late-phase airway response; mAb, monoclonal antibody; MUC5AC, mucin 5AC protein isoform; pEGFR, phosphorylated EGFR; 44/42MAPK, mitogen-activated protein kinase isoform 44/42; pMAPK phosphorylated MAPK; R_L, pulmonary-flow resistance; ROS, reactive oxygen species; RU, resonance units; SPR, surface plasmon resonance.

[1] To whom correspondence should be sent (email dsexton@dyax.com).

could be an effective therapeutic strategy for respiratory diseases.

KLK1 has been reported to be the primary kininogenase in the airways, and its activity is elevated in BAL (bronchoalveolar lavage) fluid from patients with asthma and allergic rhinitis and its levels increase even further after allergen challenge [22,23]. However, plasma kallikrein, another potent kininogenase, is expressed by epithelial cells of the lung, so it could potentially contribute kininogenase activity in allergic airways [24]. In airway secretions from patients undergoing mechanical ventilation, KLK1 activity has also been reported to be elevated [25]. Similar to the role of other tissue kallikreins in pro-hormone and growth-factor activation [26], KLK1 has also been shown to cleave membrane-bound EGF (epidermal growth factor) from human airway epithelial cells [15]. EGF shedding by KLK1 leads to EGFR (EGF receptor) activation, which induces mucus hypersecretion and goblet-cell hyperplasia, which are characteristics of chronic bronchitis [27].

We previously described the discovery of anti-KLK1 human antibodies using a high-diversity phage-display library in combination with a high-throughput SPR (surface plasmon resonance) affinity screening method [28,29]. In the present study we demonstrate that one of these human antibodies, DX-2300, is a potent and highly specific competitive inhibitor of KLK1. We show that DX-2300 blocks EGFR activation and mucus-cell proliferation in HBE (human tracheobronchial epithelial) cells, as well as bronchoconstriction and AHR (airway hyper-responsiveness) in a sheep model of asthma. Our data support previous reports [22,23] that KLK1 is the primary kininogenase in the airways.

EXPERIMENTAL

Materials

All chemicals were of the highest available quality and were obtained from Sigma–Aldrich unless indicated otherwise. KLK1 and the other tissue kallikreins were obtained from R&D Systems and assayed according to the suggested protocol of the manufacturer. Human plasma kallikrein was obtained from Enzyme Research Laboratories. Human trypsin, human plasmin, human neutrophil elastase, human chymotrypsin and human thrombin were obtained from Athens Research and Technology. Human urokinase-type plasminogen activator, tissue plasminogen activator and activated Protein C were obtained from Calbiochem. Human tryptase was obtained from Fitzgerald Industries. *H*-D-Pro-Phe-Arg-chloromethylketone was obtained from Bachem Biosciences Inc. CM5 biosensor chips were obtained from Biacore. Bradykinin ELISA measurements were performed using a commercially available kit according to the instructions of the manufacturer (Bachem Biosciences Inc.). Soluble EGF levels were assessed using a commercially available ELISA kit (Quantikine; R&D Systems).

Antibody expression and purification

Anti-KLK1 antibodies were discovered using phage display as previously described [29]. The Fab version of DX-2300 was converted into full-length human IgG1 antibodies as previously described [30] and expressed in CHO (Chinese-hamster ovary) cells using a fed-batch fermentation strategy. Harvested cell-culture medium was passed through two depth filters, followed by sterile filtration through a 0.2-μm-pore-size membrane (Millipore). mAb (monoclonal antibody) in the clarified medium was then captured by Mabselect ProA (GE Healthcare) chromatographic process, followed by anion-exchange chromatography using UNO-Q resin from Bio-Rad and cation-exchange chromatography using Toyopearl SP-650M resin from Tosoh Bioscience. The purified IgG1 was buffer-exchanged by ultrafiltration/diafiltration through a 30-kDa-cut-off membrane from Millipore into a buffer [100 mM citrate/phosphate buffer, pH 6.0, 50 mM NaCl, 2 % (w/v) trehalose and 0.01 % Tween-80]. Purified DX-2300 IgG1 was analysed by analytical size-exclusion chromatography using a G3000SWXL column from Tosoh Bioscience and shown to contain less than 5 % high-molecular-mass aggregates. Contaminants such as leached Protein A, double-stranded DNA, host-cell protein and endotoxin were all below acceptable limits for *in vivo* studies. The A2 isotype control antibody is a human IgG1 that was also discovered by phage display using streptavidin as the antigen. This control antibody was expressed and purified similarly to DX-2300.

In vitro kinetic assays of DX-2300

KLK1 (total protein concentration 0.5 nM) was incubated either in the absence of DX-2300 or with 11 different concentrations of DX-2300 (maximum concentration 5.5 nM; minimum concentration 0.095 nM; serial dilution 2/3) for 2 h in reaction buffer {20 mM Tris/HCl, pH 7.5, 150 mM NaCl, 1 mM EDTA, 0.1 % PEG [poly(ethylene glycol)]-8000 and 0.1 % Triton X-100} in a volume of 90 μl in a well of a 96-well plate. To each inhibitor dilution series, 10 μl of a solution of a synthetic peptide substrate [Pro-Phe-Arg-AMC (Pro-Phe-Arg-7-amido-4-methylcoumarin); Sigma–Aldrich; final maximum concentration 200 μM; final minimum concentration 26.3 μM; serial dilution 2/3] was added to a well of a 96-well plate. Fluorescence measurements were obtained using a fluorescence plate reader (Gemini; Molecular Devices) with excitation and emission wavelengths set at 360 nm and 460 nm respectively.

Initial reaction rates were determined by non-linear regression of the progress curves. Plots of initial reaction rate versus DX-2300 concentration were globally fitted [31] to a system of simultaneous non-linear algebraic equations corresponding to the given inhibition mechanism, according to an rapid-equilibrium algorithm [32] using the software DYNAFIT [33] (BioKin Ltd.). Model discrimination analysis was performed using the second-order AIC_c (Akaike Information Criterion) [34]. Non-symmetrical confidence intervals for model parameters were estimated using the profile-t method [35]. Details of model selection and confidence-interval estimation are shown in the accompanying Supplementary Online Material (at http://www.BiochemJ.org/bj/422/bj4220383add.htm).

SPR analysis

SPR measurements were performed using a Biacore 3000 instrument. Goat anti-human Fc-fragment-specific IgG (Jackson ImmunoResearch Laboratories) was immobilized by amine coupling on a CM5 sensor chip at an immobilization density of approx. 7000 RU (resonance units). The reference flow cell was activated and blocked in a mock amine-coupling reaction. DX-2300 was captured on the derivatized flow cell by injecting a 50 nM solution of antibody for 1 min at 5 μl/min. Untreated KLK1, or KLK1 which had been pre-incubated with AEBSF [4-(2-aminoethyl)benzenesulfonyl fluoride hydrochloride] or *H*-D-Pro-Phe-Arg-chloromethane, was then injected as indicated over captured DX-2300 for 5 min at a flow rate of 50 μl/min. The sensor chip surface was regenerated with a 30 s pulse of 10 mM glycine, pH 1.5, at a flow rate of 100 μl/min. Measurements were

performed at 25 °C using HBS-P (10 mM Hepes, pH 7.4, 150 mM NaCl and 0.005 % surfactant P20) as the running buffer.

Measurements of KLK1 activity in biological samples

Human urine and saliva were obtained from healthy volunteers with their informed consent. Saliva was collected using a Salivette device according to the instructions of the manufacturer (Sarstedt). Mouse urine was obtained from Golden West Biologicals. Sheep urine was obtained using a catheter. All protocols involving animals used in the present study were approved by the Mount Sinai Medical Center Animal Research Committee, which is responsible for assuring the humane care and use of experimental animals. Human plasma and serum were obtained from Sigma. Human BAL fluid was obtained, with informed consent, from four asthmatic patients with a rhinitis infection. KLK1-like activity was measured by diluting each sample, other than BAL fluid, 1:10 in reaction buffer and using Pro-Phe-Arg-AMC as the substrate at a concentration of 100 μM in the presence of 5 μM soybean trypsin inhibitor, which was added to inhibit trypsin-like protease activity not due to KLK1. KLK1-like activity was measured in BAL fluid by adding 80 μl of BAL fluid to 10 μl of 10 × reaction buffer and 10 μl of 1 mM Pro-Phe-Arg-AMC as the substrate in the presence of 5 μM soybean trypsin inhibitor. KLK1 activity in the cell culture supernatant from ALI (air/liquid interface) cultures was measured using Val-Leu-Arg *p*-nitroanilide as the substrate at a concentration of 1 mM. The activity in ALI cultures was expressed as μg of KLK1 per mg of total protein. The mass of KLK1 in the ALI cultures was determined using a KLK1 standard curve using purified recombinant KLK1 as previously described [15]. Total protein was measured using the BCA (bicinchoninic acid) assay (Thermo Scientific).

Primary cultures of HBE cells grown at the ALI

Primary cultures of HBE cells were obtained from human lung donors (with informed consent), through the University of Miami Life Alliance Organ Recovery Agency with approval from the local Institutional Review Board. HBE cells were harvested as described in [27] and were plated on collagen-coated plastic dishes, grown to confluence to yield undifferentiated airway epithelial cells and passaged after enzyme dissociation with trypsin. Cells from passage 1 were plated on to 24-mm-diameter Transwell clear culture inserts (Corning Costar Corporation) coated with human placental collagen. The apical surface was exposed to air as soon as the cells reached confluence. Cultures were used for experiments after reaching full differentiation (3 weeks on air) as assessed by visual confirmation of beating cilia and mucus. The cultures used in this study had 89 $\pm$ 4 % of ciliated cells ($n = 10$ lung donors) measured by labelling ciliated cells with an anti-(acetylated tubulin) mAb and analysed using Metamorph software (Universal Imaging Corporation) as described below.

Immunoassays

Soluble EGF levels were assessed using a commercially available ELISA kit (Quantikine; R&D Systems). EGFR activation was assessed as previously described [15]. Briefly, two aliquots of cell lysates (three different lung donors) containing equal amounts of protein were used for estimating total and pEGFR (phosphorylated EGFR) on parallel Western blots. EGFR was immunoprecipitated using a rabbit anti-EGFR antibody (1 μg/ml; Santa Cruz Biotechnology) and Protein A–agarose beads (Santa Cruz Biotechnology). Pellets from immunoprecipitation were electrophoresed on Tris/HCl/4–15%-(w/v)-polyacrylamide Ready Gels (Bio-Rad) and transferred electrophoretically to PVDF membranes (Millipore). The membranes were blocked with 1 % gelatin in TBS (Tris-buffered saline; 20 mM Tris/HCl and 150 mM NaCl, pH 7.4) containing 0.05 % Tween 20 (1 h), followed by an anti-phosphotyrosine mAb (PY99, 2 μg/ml; Santa Cruz Biotechnology) or anti-EGFR mAb (Ab-3, 1 μg/ml; Calbiochem). The secondary antibody was an alkaline-phosphatase-conjugated goat anti-mouse IgG (0.5 μg/ml, KPL Inc.). For visualization, bromochloroindolyl phosphate/Nitro Blue Tetrazolium was used as a substrate. Developed blots were photographed using the GelDoc XRS system (Bio-Rad), and quantification of the pEGFR/EGFR ratio was done using Quantity One software (Bio-Rad).

Visualization of 44/42MAPK (mitogen-activated protein kinase isoform 44/42) and pMAPK (phosphorylated MAPK) was achieved using the PhosphoPlus p44/p42 MAPK (Thr^{202}/Thr^{204}) kit according to the manufacturer's instructions (Cell Signaling Technology).

Goblet-cell quantification

Goblet-cell hyperplasia was assessed as previously described [27]. Briefly, the apical surface of HBE cells was gently rinsed with PBS (37 °C) to remove mucus and debris. Cells were fixed with acetone/methanol (1:1, v/v) for 1 min. After fixation, cells were blocked with 1 % BSA in PBS and labelled with 10 μg/ml anti-MUC5AC [anti-(mucin 5AC protein isoform)] antibody (Chemicon International). Relative quantification of MUC5AC-positive cells was done using the Metamorph software. Results were expressed as fold increase of the number of positive MUC5AC cells/field over the control values obtained with PBS treatment.

In vivo studies

The allergic sheep (27–50 kg body weight) used had previously been shown to develop both early and late bronchial responses to inhaled *Ascaris suum* (nematode worm) antigen. Sheep were conscious and were restrained in a cart in the prone position with their heads immobilized. Breath-by-breath determination of mean R_L (pulmonary flow resistance) was measured with the oesophageal-balloon technique [36]. All aerosols were generated using a disposable medical nebulizer (Raindrop®; Nelcor–Puritan Bennett). Airway responsiveness was determined from cumulative concentration–response curves to carbachol inhaled as previously described [36]. R_L was measured immediately after inhalation of PBS and after each consecutive administration of ten breaths of increasing concentrations of carbachol [0.25, 0.5, 1.0, 2.0 and 4.0 % (w/v) in PBS]. The provocation test was discontinued when the R_L increased over 400 % from the post-PBS value or after the highest carbachol concentration had been administered. The cumulative carbachol concentration [in BU (breath units)] that increased R_L by 400 % over the post-PBS value (PC_{400}) was calculated by interpolation from the dose–response curve. One BU was defined as one breath of a 1 % (w/v) carbachol aerosol solution [36]. BAL fluid was obtained as previously described [36].

RESULTS

DX-2300 *in vitro* inhibition mechanism

The *in vitro* inhibition mechanism of DX-2300 and the associated kinetic constants were determined from a collection of 72 continuous assays conducted at six different substrate concentrations

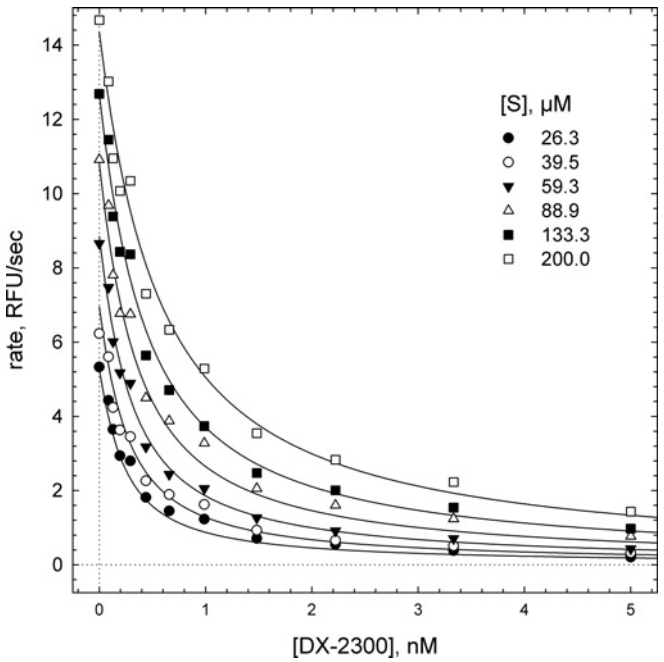

Figure 1 *In vitro* inhibition of KLK1 by DX-2300

Initial rates were determined from continuous assays as described in the Experimental section. The smooth curves (global fit of all displayed data) represent the competitive inhibition model, defined as a system of simultaneous non-linear algebraic equations automatically derived by the software DYNAFIT [32,33]. The best-fit values of kinetic constants and the enzyme concentration to a competitive inhibition mechanism (see the Supplementary Online Material) are $K_i = 0.13 \pm 0.01$ nM, $K_s = 71 \pm 9$ μM and [E] (enzyme concentration) $= 0.11 \pm 0.05$ nM. Abbreviation: RFU, relative fluorescence unit.

(Figure 1). A model discrimination analysis was performed by examining four standard inhibition mechanisms: (1) competitive; (2) uncompetitive; (3) pure non-competitive; and (4) mixed-type non-competitive (see the Supplementary Online Material). In the first round of model discrimination analysis, the competitive mechanism and the mixed-type non-competitive mechanism were ranked as equally plausible; the uncompetitive and pure non-competitive mechanisms were clearly excluded. In the second round of model discrimination analysis, we examined the non-symmetrical confidence intervals, at the 99 % probability level, for inhibition constants appearing in the competitive and mixed-type mechanisms. The confidence interval for the inhibition constant, K_i, in the competitive model was $K_i = 0.11$–0.16 nM. The best-fit value for K_i in the mixed-type non-competitive model was $K_i = (0.12 - 0.25)$ nM, but the confidence interval for the inhibition constant, K_{is} (see the Supplementary Online Material), was open-ended, with $K_{is} = 0.6$–∞ nM. An asymptotically infinite value of K_{is}, within the 99 % probability level, means that there is no binding of DX-2300 to the Michaelis complex and that the inhibitor binds only to the free enzyme. We conclude that DX-2300 is a kinetically competitive inhibitor of KLK1, with the best-fit value of $K_i = 0.13$ nM.

Using an SPR biosensor assay we observed that DX-2300 does not bind the complex formed between KLK1 and known active-site inhibitors (Figure 2). AEBSF and *H*-D-Pro-Phe-Arg-chloromethane are active-site-directed covalent inhibitors of KLK1. The inability of DX-2300 to bind either KLK1 covalently modified with AEBSF or *H*-D-Pro-Phe-Arg-chloromethane suggests that DX-2300 binds at or near the active site of the enzyme. This finding is consistent with a competitive inhibition mechanism.

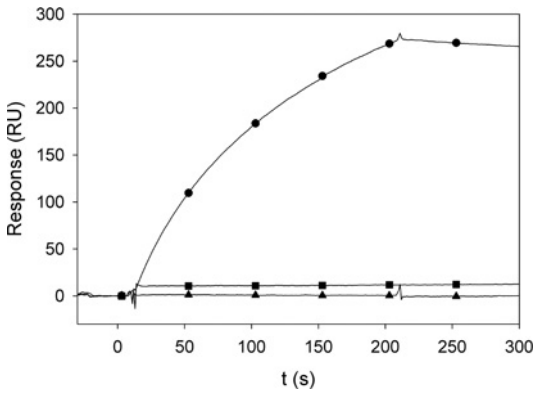

Figure 2 SPR analysis of DX-2300 binding to active site blocked KLK1

DX-2300 was immobilized on a CM5 sensor chip through capture with an anti-(human Fc) specific antibody. KLK1 (100 nM; ●) or KLK1 pretreated with either 1 mM AEBSF (100 nM; ■) or 1 mM *H*-D-Pro-Phe-Arg-chloromethane (▼) was flowed over the chip.

DX-2300 is a specific KLK1 inhibitor

To evaluate the inhibition specificity of DX-2300, we tested whether the antibody inhibited various serine proteases, including 11 different human tissue kallikreins. At the maximum concentration that was tested (1 μM) we found that DX-2300 did not inhibit any of the proteases that were tested: plasma kallikrein, trypsin, plasmin, urokinase-type plasminogen activator, tissue plasminogen activator, neutrophil elastase, activated protein C, chymotrypsin, thrombin, tryptase and all commercially available active human tissue kallikreins (KLK2, KLK3, KLK4, KLK5, KLK6, KLK7, KLK8, KLK11, KLK12, KLK13 and KLK14) (results not shown). Preparations of active KLK9, KLK10, and KLK15 were not available for testing. The lack of inhibition of any tested protease by DX-2300 indicates that this antibody is highly specific for tissue kallikrein inhibition.

DX-2300 inhibits KLK1 activity in biological samples

To validate the use of DX-2300 for specific KLK1 inhibition, we measured the inhibition of KLK1-like activity in biological samples known to either contain, or be deficient in, active KLK1. KLK1 has been previously demonstrated to be responsible for the kallikrein-like activity observed in urine, saliva and asthmatic BAL fluid [13,14,22]. The percentage of KLK1-like activity inhibited by DX-2300 is plotted for each sample in Figure 3. KLK1 is present in urine because it is secreted from epithelial cells in the distal tubule of the kidney [13]. DX-2300 completely inhibited the observed KLK1-like activity in human and sheep urine. However, DX-2300 did not inhibit the KLK1-like activity in mouse urine – a result consistent with the observation that the antibody does not inhibit recombinant mouse Klk1 (results not shown). KLK1 is secreted into saliva from the submandibular gland [14]. DX-2300 completely inhibited the KLK1-like activity in human saliva (Figure 3). Active KLK1 is not expected to be present in measurable quantities in serum or plasma, since previous reports indicate that, unlike plasma kallikrein, which circulates as a zymogen in plasma concentrations of approx. 500 nM, KLK1 is present in the circulation mainly as an inactive proenzyme bound to the extracellular surface of neutrophils via cell-associated HMMK [37]. The observation that DX-2300 did not inhibit the KLK1-like activity in human serum or plasma suggests that the activity in these samples is attributed to other proteases capable of hydrolysing the synthetic substrate. Human BAL fluid from

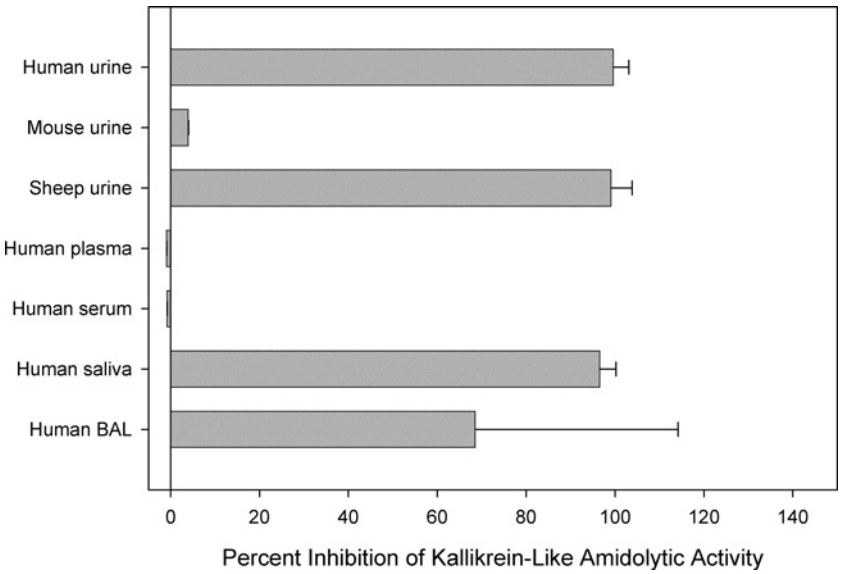

Figure 3 DX-2300 inhibition of KLK1-like activity in biological samples

Samples were diluted and assayed as described in the Experimental section in the presence or absence of 1 μM DX-2300. The rates were expressed as percentage inhibition, calculated as follows: inhibition (%) = [(100–observed rate in the presence of DX-2300)/(rate in the absence of DX-2300)] $\times$ 100.

asthmatic patients has been previously shown to contain active KLK1 [22]. We found that DX-2300 inhibited the KLK1-like activity towards the synthetic substrate in human BAL fluid by about 70 %. However, using a bradykinin ELISA, the kininogenase activity in human BAL fluid (36 ± 15 ng of bradykinin/mg of total protein) was completely inhibited by 100 nM DX-2300 (0.15 ± 0.22 ng of bradykinin/mg of total protein). The observation that DX-2300 inhibits the KLK1-like activity in human and sheep urine as well as human saliva suggests that KLK1 is the main protease in these tissue samples capable of hydrolysing the Pro-Phe-Arg-AMC substrate. By contrast, human BAL fluid appears to contain other proteases at similar levels to KLK1 that can hydrolyse the synthetic substrate. However, the results from the bradykinin ELISA suggest that KLK1 is the main kininogenase present in BAL fluid, a result consistent with previous observations [22,38].

DX-2300 blocks ROS (reactive oxygen species)-induced EGF activation and EGFR signalling in HBE cells grown at the ALI

We previously showed that oxidative-stress-induced EGFR activation and mucus hypersecretion was mediated by the protease activity of KLK1 [15]. As shown in Figure 4, exposure of HBE cells to ROS resulted in a significant increase in the amount of active KLK1 in the cell culture medium (0.51 ± 0.03 μg/mg of protein) compared with PBS-treated control cells (1.46 ± 0.12 μg/mg of protein), which was blocked by pretreatment with DX-2300 (0.08 ± 0.01 μg/mg of protein). ROS-treated HBE cells also exhibited increased EGF in the cell culture medium (2.02 ± 0.32 pg/mg of protein) compared with PBS-treated control cells (5.92 ± 1.30 pg/mg of protein), which was blocked by pretreatment with DX-2300 (1.73 ± 0.32 pg/mg of protein; Figure 4B).

DX-2300 blocked EGFR downstream activation, as assessed by MAPK phosphorylation (Figure 5) and HBE cell hyperplasia (Figure 6). Once-daily xanthine/xanthine oxidase treatment for 3 days increased the percentage of MUC5AC-positive cells (32.3 ± 8.7 %) as compared with PBS-treated cells (5.2 ± 4.0 %)

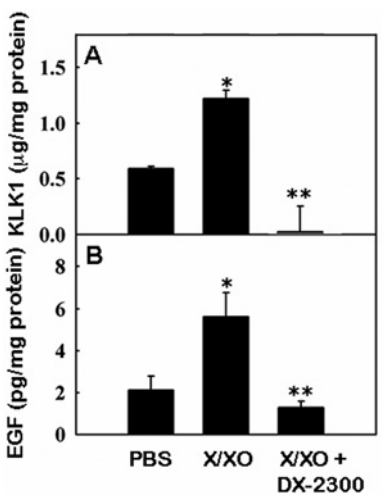

Figure 4 DX-2300 blocks ROS-induced KLK1 secretion and EGF shedding from HBE cells

(**A**) ROS-induced KLK1 release; (**B**) ROS-induced EGF release. Values in treated groups were compared with the PBS-treated group to obtain *P* values using a two-tailed unpaired heteroscedastic Student's *t* test (*$P < 0.05$; **$P < 0.001$).

(Figure 6). This increase in the number of HBE mucous cells was inhibited by DX-2300 (11.4 ± 2.1 %), which is consistent with a mechanism whereby DX-2300 blocks ROS-induced EGF shedding and EGFR activation.

Effect of KLK1 inhibition on pulmonary function in allergen-challenged allergic sheep

Since DX-2300 inhibits sheep KLK1, we used a sheep model of asthma to investigate the effect of specific inhibition of KLK1 on airway function. When DX-2300 was administered either by inhalation (10 mg at both 12 h and at 30 min prior to challenge with allergen; Figure 7) or intravenously (up to 12 mg/kg;

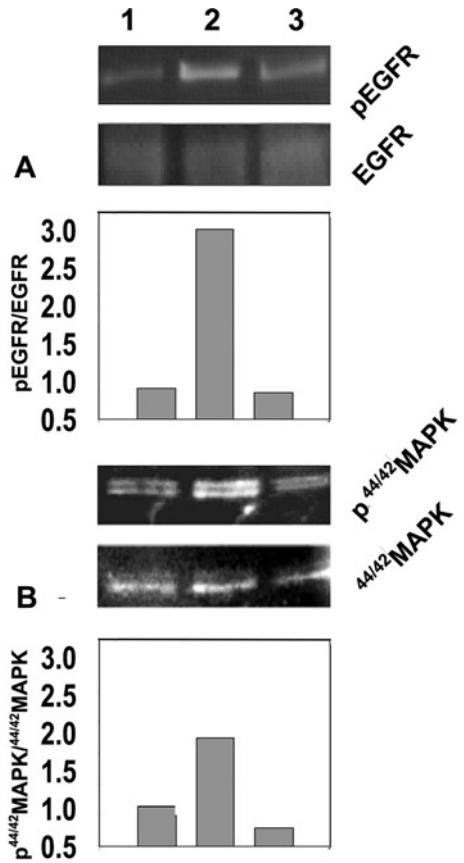

Figure 5 DX-2300 blocks ROS-induced EGFR activation and downstream signalling

HBE cells grown at the ALI were exposed to (1) PBS; (2) xanthine/xanthine oxidase (X/XO); or (3) xanthine/xanthine oxidase after DX-2300 pretreatment (1 μg/ml). (**A**) Top two panels: pEGFR and total EGFR were detected using specific antibodies as described in the Experimental section; bottom panel: pEGFR/EGFR ratios assessed by densitometry. (**B**) Top two panels: p44/42MAPK and total MAPK detected as described in the Experimental section; bottom panel: p44/42MAPK and total MAPK ratios assessed by densitometry [15].

Table 1), we observed no effect on the EAR (early-phase airway response), but a marked inhibition of LAR (late-phase airway response). In the aerosol studies, sheep treated with an isotype control mAb (A2) exhibited a LAR that began approx. 4 h after challenge and reached an increase in lung resistance to approx. 120 % at 8 h post-challenge (Figure 7 and Table 1).

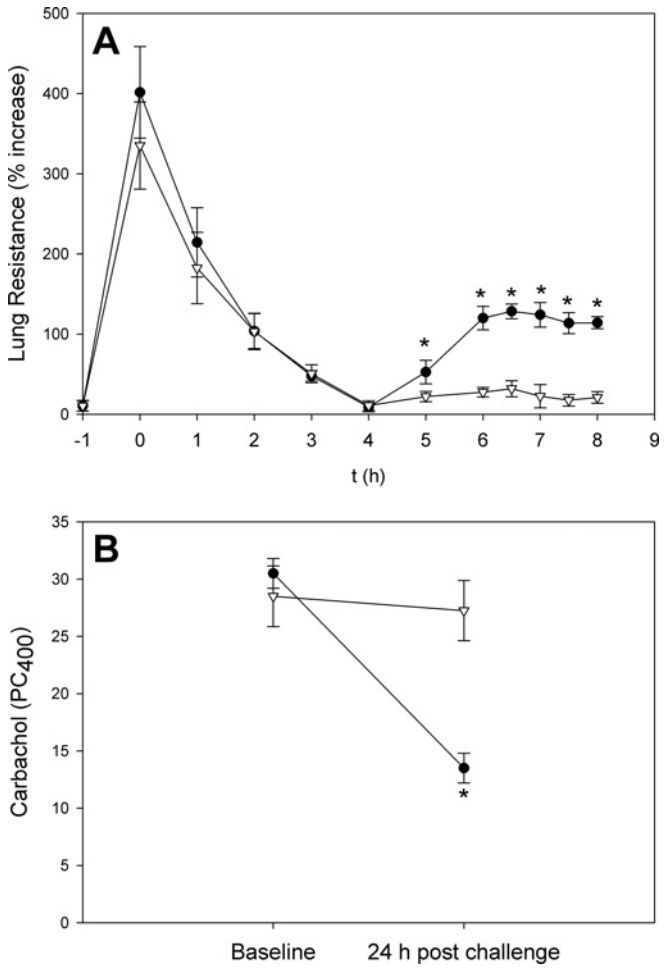

Figure 7 Effect of DX-2300 on allergen-induced bronchoconstriction and AHR

(**A**) Lung resistance was measured following the administration of *A. suum* allergen to sheep treated with an isotype-inactive antibody A2 ($n = 4$; ●, control) or sheep treated with two 10 mg inhaled doses of DX-2300 ($n = 4$; ▽). Sheep were treated with 10 mg of inhaled DX-2300 at 12 h and at 30 min prior to challenge with *A. suum* allergen. (**B**) AHR to inhaled carbachol was determined by measuring the amount of carbachol in BU (see the Experimental section) required to induce a 400 % increase in bronchoconstriction (PC_{400}). PC_{400} values were measured before allergen challenge and 24 h after allergen challenge in the same sheep used to obtain lung function measurements (**A**) that were either treated with the inactive antibody (●) or treated with DX-2300 (▽). Values in the treated group with P values < 0.001 when compared with the control treated group are indicated (*). A two-tailed unpaired heteroscedastic Student's t test was used to calculate P values.

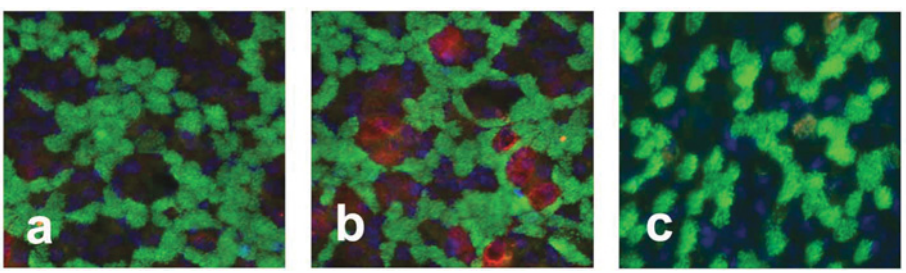

Figure 6 DX-2300 prevents HBE-cell hyperplasia induced by chronic exposure to ROS

HBE cellsgrown at the ALI were treated with either PBS (**a**) or with xanthine/xanthine oxidase (**b**, **c**) in the absence (**b**) or presence (**c**) of DX-2300 (1 μg/ml) for 3 consecutive days. Goblet cells were visualized by immunofluorescence by labelling MUC5AC (red) and ciliated cells by labelling acetylated tubulin (green). Nuclei were visualized with 4′,6-diamidino-2-phenylindole ('DAPI'). Images were obtained by confocal microscopy (original magnification 63 ×).

Table 1 Summary of lung function measurements in DX-2300-treated sheep

Each of the intravenously treated groups contained two animals. Four animals were used in the groups that received either DX-2300 or the A2 control antibody by inhalation.

DX-2300 treatment	Time of treatment (prior to challenge)	EAR (% inhibition)*	LAR (% inhibition)†	PC ratio + drug‡	PC ratio + vehicle
Intravenous					
1.2 mg/kg	30 min	11	–7	0.45	0.52
6 mg/kg	30 min	–2	41	0.77	0.54
12 mg/kg	30 min	12	72	0.74	0.49
2 × 12 mg/kg	24 h and 30 min	–16	77	0.89	0.55
By inhalation					
2 × 10 mg	24 h and 30 min	11	91§	0.96	0.44

* The percentage inhibition of the EAR is calculated by determining the AUC from 0 to 4 h (see Figure 8A) for vehicle- versus drug-treated animals and expressing it as a percentage (see the equation in the text).

† The percentage inhibition of LAR was calculated by determining the AUC from 4 to 8 h for vehicle- versus drug-treated animals and expressing it as a percentage as was done for the EAR.

‡ The PC ratio is the provocative challenge ratio of the carbachol PC_{400} values obtained for post-allergen challenge divided by the prechallenge PC_{400}; a PC ratio below 1.0 indicates the development of AHR.

§ The EAR (% inhibition) and LAR (% inhibition) for inhaled DX-2300 was calculated using the A2 control antibody as the vehicle response.

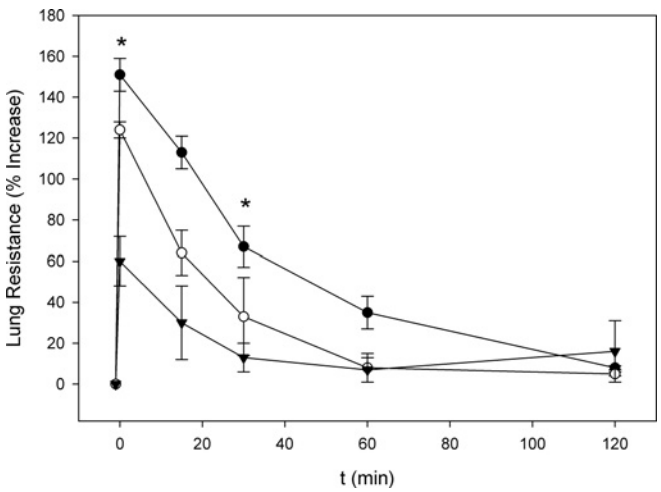

Figure 8 Effect of DX-2300 on kininogen-induced bronchoconstriction

Lung resistance was measured following the administration of HMMK (100 μg) to sheep not treated with DX-2300 ($n = 4$; ●) or sheep treated with either 1 mg of inhaled DX-2300 ($n = 2$; ○) or 5 mg of DX-2300 ($n = 2$; ▼). Sheep were treated with inhaled DX-2300 30 min prior to challenge with HMMK. Lung-resistance values in the 5 mg treatment group with P values < 0.001 when compared with the untreated group are indicated (*). A two-tailed unpaired heteroscedastic Student's t test was used to calculate P values.

As shown in Figure 8(A), two inhaled 10 mg doses of DX-2300 (at 12 h and at 30 min prior to challenge) blocked the onset of LAR by 91 % (Figure 7 and Table 1). When DX-2300 was administered intravenously, we observed that the 1.2 mg/kg dose was ineffective and the 6 mg/kg dose had an intermediate effect on LAR, whereas both the 1 × 12 mg/kg dose and the 2 × 12 mg/kg dose were more effective in blocking LAR (Table 1) compared with the control (untreated) sheep.

At 24 h after allergen challenge, airway responsiveness to carbachol was measured to determine whether the animals developed AHR. Inhalation of two 10 mg doses of DX-2300 (12 h and 30 min prior to challenge) resulted in approximately the same PC_{400} value before and after allergen challenge (Figure 7B; PC ratio = 0.96 in Table 1). Consequently, this inhaled dosing regimen appears to completely block the development of AHR. In contrast, sheep treated with inhaled A2 isotype control had a 56 % lower PC_{400} value after challenge as compared with pre-challenge measurements, indicating the development of AHR (Figure 7B; PC ratio = 0.44 in Table 1). Intravenously administered DX-2300, at the 1.2 mg/kg dose, did not protect the development of AHR (PC ratio = 0.45), whereas the 6 mg/kg dose, the 1 × 12 mg/kg dose and the 2 × 12 mg/kg dose attenuated the development of AHR (PC ratios > 0.74; Table 1).

BAL fluid was collected 24 h after allergen challenge from sheep treated with either inhaled DX-2300 or inhaled A2 isotype control antibody for the measurement of inflammatory cell influx. As shown in Table 2, allergen challenge was associated with an increased number of inflammatory cells relative to the number in the unchallenged sheep lung. Sheep treated with inhaled DX-2300 did not have statistically reduced levels of inflammatory cells in BAL fluid 24 h after allergen challenge (Table 2). However, fewer neutrophils were measured in the allergen-challenged BAL fluid of DX-2300 treated animals [$(8 \pm 2.1) \times 10^3$ cells/ml] than in the BAL fluid from control antibody-treated animals [$(56 \pm 2.1) \times 10^3$) cells/ml].

Previously, the administration of inhaled HMMK to allergic sheep was shown to induce bronchoconstriction that was blocked by α_2-proteinase inhibitor, which is an inhibitor of KLK1, or by a B2 receptor antagonist [36,39]. Since HMMK is a substrate for KLK1, it was instructive to investigate whether a specific KLK1 inhibitor, such as DX-2300, would also block HMMK-induced bronchoconstriction. As shown in Figure 8, the inhalation of either 1 or 5 mg of DX-2300 inhibited HMMK-induced bronchoconstriction by 49 and 68 % respectively. The percentage inhibition was calculated by determining the AUC (area under the curve) for each plot in Figure 8:

$$\text{Inhibition (\%)} = \left[\frac{100 - \text{AUC}_{\text{drug-treated}}}{\text{AUC}_{\text{vehicle-treated}}}\right] \times 100$$

DISCUSSION

Inhibitors of KLK1 have been shown to be efficacious in animal models of tissue oedema, cancer invasiveness, acute pancreatitis and airway inflammation [40–44]. DX-2300 is the first fully human antibody inhibitor of KLK1 that has been reported and is among the most potent and specific inhibitors of KLK1. Its competitive inhibition mechanism and its inability to bind KLK1 complexed with active-site inhibitors suggest that DX-2300 binds an epitope at or near the KLK1 active site. In the present study we used this antibody to quantify KLK1 in crude biological samples

Table 2 Effect of DX-2300 on inflammatory cell influx in BAL fluid from allergic sheep

Allergic sheep ($n = 4$) were treated by inhalation with two 10 mg doses of either A2 antibody or DX-2300, 12 hours and 30 minutes prior to challenge with *A. suum*. BAL was obtained as described in the Experimental section.

	10^{-3} × Cell concentration (number of cells/ml)			
	A2 antibody isotype control		DX-2300	
Cell type	Before challenge	24 h post challenge	Before challenge	24 h post challenge
Total	204 ± 25	331 ± 40	182 ± 13	266 ± 53
Macrophages	162 ± 12	228 ± 20	154 ± 10	233 ± 48
Lymphocytes	32 ± 16	38 ± 9	22 ± 4	22 ± 6
Neutrophils	1.2 ± 0.8	56 ± 28	1.8 ± 1	8 ± 2.1*
Eosinophils	6 ± 3	4.6 ± 1.4	1.4 ± 0.3	1.3 ± 0.7

*$P = 0.18$ versus the neutrophil count in the A2-antibody-treated sheep at 24 h post challenge; A two-tailed unpaired heteroscedastic Student's t test was used to calculate P values.

and confirmed its ability to inhibit KLK1-mediated responses *in vitro* using primary cultures of HBE cells and kinin generation *in vivo* in a sheep model of asthma.

The high specificity of DX-2300 can be used to confirm the presence of KLK1 activity in complex biological samples. The presence of KLK1 activity in a crude sample that contains other proteases can be identified by the ability of DX-2300 to inhibit the observed KLK1-like activity. We used DX-2300 to confirm that KLK1 is secreted from HBE cells after exposure to ROS and is responsible for EGF shedding and downstream EGFR activation – results that support previous findings [15,27]. Treating HBE cells with DX-2300 prior to ROS exposure blocked EGFR activation and subsequent mucus hypersecretion. These results are consistent with KLK1 being the protease responsible for pro-EGF cleavage from epithelial-cell surfaces, which leads to EGFR activation, mucus hypersecretion and goblet-cell hyperplasia, as previously described [15,27].

In vivo models of asthma have previously implicated the kallikrein–kinin system in disease pathology. KLK1 inhibitors, as well as B1 and B2 receptor antagonists, show efficacy in various animal models of asthma [45]. We tested DX-2300 in the sheep model of asthma because DX-2300 cross-reacts with sheep KLK1. Furthermore, the sheep model offers the ability to measure pulmonary function using procedures similar to those that have been performed in humans [46,47]. KLK1-like activity was shown to be elevated in BAL fluid from allergic sheep after challenge with either inhaled allergen, xanthine/xanthine oxidase, elastase or HMMK [36]. α_2-Proteinase inhibitor is a protein inhibitor of serine proteases, including KLK1, that blocks AHR in sheep [36].

We observed that sheep treated with DX-2300 exhibited decreases in both allergen-induced late-phase bronchoconstriction and the AHR to carbachol that was observed 24 h after allergen challenge. DX-2300 did not block the EAR, which is mediated by mast-cell degranulation and the release of mediators such as histamine, cysteinyl-leukotrienes and prostaglandin D_2. The release of these mediators is not dependent upon the kallikrein–kinin system, so a specific KLK1 inhibitor would not be expected to affect the EAR. Although the EAR is associated with the first signs of an asthmatic attack, it is usually controlled by short-acting β-adrenergic agents. When it is not controlled, it is due to an underlying inflammation that is associated with asthma exacerbations. Thus it is important to control the subsequent inflammatory processes that are triggered by an allergic episode. The LAR and subsequent AHR are physiological indicators of the underlying inflammation resulting from allergen challenge [46].

KLK1 activity was found to increase after the EAR, around the onset of the LAR phase, in both humans [22] and sheep [39]. Kinins generated by KLK1 in the airways would be expected to contribute to the observed bronchoconstriction associated with LAR and the ensuing inflammation leading to airway hypersensitivity (as measured by AHR). The ability of DX-2300 to block both LAR and AHR supports previous reports implicating KLK1 and the kallikrein–kinin system in airway inflammation [18,19]. Furthermore, the observation that ROS liberate KLK1 from epithelial cells also supports a role for KLK1 in airway inflammation, since ROS are generated after the EAR. If an asthmatic has an exacerbation during the period when their airways are inflamed, the exacerbation is usually more easily precipitated and the severity is worse, as evidenced by AHR. Attenuating airway inflammation with a KLK1 inhibitor may lessen the severity of subsequent attacks.

The efficacy of a specific KLK1 inhibitor in this model demonstrates that KLK1 is the primary kininogenase in sheep airways. Plasma kallikrein has been previously shown to be present in lung epithelial cells [24] and could therefore contribute to kininogenase activity in the airways. Plasma kallikrein could also enter the lung after allergen challenge as part of plasma leakage. However, since DX-2300 does not block plasma kallikrein, our data indicate that KLK1 is the primary kininogenase in the lung. Interestingly, the inhalation of kininogen (HMMK) causes bronchoconstriction in allergic sheep to a level that approximates to that observed during late-phase bronchoconstriction ($\sim 150\,\%$ increase in lung resistance). The observation that DX-2300 blocked HMMK-induced bronchoconstriction demonstrates that active KLK1 is present in airways of allergic sheep. Antigen-induced late-phase bronchoconstriction and AHR are believed to be associated with the influx of inflammatory cells into the airways.

In contrast with ovalbumin-sensitized mouse models of asthma, which are mainly associated with the infiltration of eosinophils, allergen-induced cell influx in the allergic sheep model mostly comprises neutrophils. Both eosinophils and neutrophils have been associated with asthma in humans [48]. The neutrophil influx that occurs during lung inflammation introduces kininogen associated with the cell surface [37]. The kininogen may then be cleaved by KLK1 to generate kinins and contribute to the late-phase bronchoconstriction and AHR. Although active KLK1 is present in allergic airways [22,36], the production of kinins may be limited by the availability of kininogen substrate. Data from *in vitro* and *in vivo* studies suggest that KLK1 is sequestered in an inactive complex with hyaluronan at the apical pole of airway epithelium [15]. ROS generated in response to allergen challenge or lung inflammation depolymerizes hyaluronan and release active KLK1. The results presented here are consistent with these mechanisms.

In summary, fully human antibody inhibitors of extracellular proteases, such as DX-2300, are useful tools to probe the role of

the protease in biological processes and may be further developed as therapeutic agents. An antibody inhibitor of a protease can offer high potency (i.e. $K_i < 1$ nM), exquisite specificity and have a prolonged plasma half-life. Human antibodies discovered using phage display are currently in clinical practice and in clinical trials [49]. Phage-display-derived therapeutic antibodies appear to be less immunogenic than humanized or chimaeric therapeutic antibodies, even though their heavy- and light-chain combinations are not always present in Nature [49].

The kallikrein–kinin system has been previously implicated in the pathology of airway diseases such as asthma and chronic obstructive pulmonary disease [19]. Our *in vitro* and *in vivo* studies with a specific antibody inhibitor of KLK1 support previous observations that both the kininogenase and the EGF sheddase activities of KLK1 participate in airway-disease progression. A potent antibody inhibitor of KLK1, such as DX-2300, has the potential of targeting two distinct pathological mechanisms of airway disease. There is a therapeutic antibody approved for asthma. XOLAIR® (omalizumab), a humanized antibody that binds and neutralizes human IgE, is approved for moderate to severe persistent allergic asthma, the symptoms of which are not controlled by asthma medicines termed 'inhaled corticosteroids' [50]. Therefore an antibody inhibitor of KLK1, such as DX-2300, could prove to be suitable for the treatment of the airway inflammation associated with asthma.

AUTHOR CONTRIBUTION

Daniel J. Sexton directed the study and wrote the paper, Ting Chen performed enzyme-inhibition measurements, Diana Martik performed and supervised enzyme-inhibition measurements, Petr Kuzmic analysed enzyme-inhibition measurements, Guannan Kuang performed bradykinin-ELISA measurements, Jie Chen developed the purification protocol for DX-2300, Andrew E. Nixon supervised purification, Bruce L. Zuraw gave expert advice on respiratory disease and the kallikrein–kinin system, Rosanna M. Forteza performed *in vitro* cell assays, William M. Abraham performed *in vivo* experiments in sheep and Clive R. Wood supervised all research, assisted with paper writing and gave expert advice on respiratory disease.

REFERENCES

1 Clements, J. A. (2008) Reflections on the tissue kallikrein and kallikrein-related peptidase family – from mice to men – what have we learnt in the last two decades? Biol. Chem. **389**, 1447–1454
2 Paliouras, M. and Diamandis, E. P. (2006) The kallikrein world: an update on the human tissue kallikreins. Biol. Chem. **387**, 643–652
3 Bhoola, K. D., Figueroa, C. D. and Worthy, K. (1992) Bioregulation of kinins: kallikreins, kininogens, and kininases. Pharmacol. Rev. **44**, 1–80
4 Calixto, J. B., Cabrini, D. A., Ferreira, J. and Campos, M. M. (2000) Kinins in pain and inflammation. Pain **87**, 1–5
5 Leeb-Lundberg, L. M., Marceau, F., Muller-Esterl, W., Pettibone, D. J. and Zuraw, B. L. (2005) International Union of Pharmacology. XLV. Classification of the kinin receptor family: from molecular mechanisms to pathophysiological consequences. Pharmacol. Rev. **57**, 27–77
6 Joseph, K. and Kaplan, A. P. (2005) Formation of bradykinin: a major contributor to the innate inflammatory response. Adv. Immunol. **86**, 159–208
7 Bhoola, K. D., Misso, N. L., Naran, A. and Thompson, P. J. (2007) Current status of tissue kallikrein inhibitors: importance in cancer. Curr. Opin. Invest. Drugs **8**, 462–468
8 Costa-Neto, C. M., Dillenburg-Pilla, P., Heinrich, T. A., Parreiras-e-Silva, L. T., Pereira, M. G., Reis, R. I. and Souza, P. P. (2008) Participation of kallikrein–kinin system in different pathologies. Int. Immunopharmacol. **8**, 135–142
9 Chao, J., Bledsoe, G., Yin, H. and Chao, L. (2006) The tissue kallikrein–kinin system protects against cardiovascular and renal diseases and ischemic stroke independently of blood pressure reduction. Biol. Chem. **387**, 665–675
10 Sainz, I. M., Pixley, R. A. and Colman, R. W. (2007) Fifty years of research on the plasma kallikrein–kinin system: from protein structure and function to cell biology and *in vivo* pathophysiology. Thromb. Haemostasis **98**, 77–83
11 Lauredo, I. T., Forteza, R. M., Botvinnikova, Y. and Abraham, W. M. (2004) Leukocytic cell sources of airway tissue kallikrein. Am. J. Physiol. Lung Cell. Mol. Physiol. **286**, L734–L740
12 Stadnicki, A., Chao, J., Stadnicka, I., Van Tol, E., Lin, K. F., Li, F., Sartor, R. B. and Colman, R. W. (1998) Localization and secretion of tissue kallikrein in peptidoglycan-induced enterocolitis in Lewis rats. Am. J. Physiol. **275**, G854–G861
13 Fujita, T., Ogino, M., Daigo, F., Yamaguchi, T. and Majima, M. (2006) Intracellular Ca^{2+} contributes to K^+-induced increase in renal kallikrein secretion. Int. Immunopharmacol. **6**, 1487–1495
14 Damas, J. (1996) Kallikrein and salivary secretion in rats during heat exposure. Immunopharmacology **32**, 125–127
15 Casalino-Matsuda, S. M., Monzon, M. E., Conner, G. E., Salathe, M. and Forteza, R. M. (2004) Role of hyaluronan and reactive oxygen species in tissue kallikrein-mediated epidermal growth factor receptor activation in human airways. J. Biol. Chem. **279**, 21606–21616
16 Barnes, P. J. (1992) Effect of bradykinin on airway function. Agents Actions Suppl. **38**, 432–438
17 Polosa, R., Rajakulasingam, K., Prosperini, G., Bellofiore, S., Britten, S., Milazzo, L. V. and Holgate, S. T. (1994) Effect of inhaled bradykinin on indices of airway responsiveness in asthmatic subjects. Eur. Respir. J. **7**, 1490–1496
18 Proud, D. (1998) The kinin system in rhinitis and asthma. Clin. Rev. Allergy Immunol. **16**, 351–364
19 Abraham, W. M., Scuri, M. and Farmer, S. G. (2006) Peptide and non-peptide bradykinin receptor antagonists: role in allergic airway disease. Eur. J. Pharmacol. **533**, 215–221
20 Eric, J., Gabra, B. H. and Sirois, P. (2003) Implication of the bradykinin receptors in antigen-induced pulmonary inflammation in mice. Br. J. Pharmacol. **138**, 1589–1597
21 Akbary, A. M., Wirth, K. J. and Scholkens, B. A. (1996) Efficacy and tolerability of Icatibant (Hoe 140) in patients with moderately severe chronic bronchial asthma. Immunopharmacology **33**, 238–242
22 Christiansen, S. C., Proud, D., Sarnoff, R. B., Juergens, U., Cochrane, C. G. and Zuraw, B. L. (1992) Elevation of tissue kallikrein and kinin in the airways of asthmatic subjects after endobronchial allergen challenge. Am. Rev. Respir. Dis. **145**, 900–905
23 Christiansen, S. C., Eddleston, J., Bengtson, S. H., Jenkins, G. R., Sarnoff, R. B., Turner, R. B., Gwaltney, Jr, J. M. and Zuraw, B. L. (2008) Experimental rhinovirus infection increases human tissue kallikrein activation in allergic subjects. Int. Arch. Allergy Immunol. **147**, 299–304
24 Fink, E., Bhoola, K. D., Snyman, C., Neth, P. and Figueroa, C. D. (2007) Cellular expression of plasma prekallikrein in human tissues. Biol. Chem. **388**, 957–963
25 O'Riordan, T. G., Weinstein, M. D., Abraham, W. M. and Forteza, R. (2003) Elevated tissue kallikrein activity in airway secretions from patients with tracheobronchitis associated with prolonged mechanical ventilation. Lung **181**, 237–244
26 Mason, A. J., Evans, B. A., Cox, D. R., Shine, J. and Richards, R. I. (1983) Structure of mouse kallikrein gene family suggests a role in specific processing of biologically active peptides. Nature **303**, 300–307
27 Casalino-Matsuda, S. M., Monzon, M. E. and Forteza, R. M. (2006) Epidermal growth factor receptor activation by epidermal growth factor mediates oxidant-induced goblet cell metaplasia in human airway epithelium. Am. J. Respir. Cell Mol. Biol. **34**, 581–591
28 Hoet, R. M., Cohen, E. H., Kent, R. B., Rookey, K., Schoonbroodt, S., Hogan, S., Rem, L., Frans, N., Daukandt, M., Pieters, H. et al. (2005) Generation of high-affinity human antibodies by combining donor-derived and synthetic complementarity-determining-region diversity. Nat. Biotechnol. **23**, 344–348
29 Wassaf, D., Kuang, G., Kopacz, K., Wu, Q. L., Nguyen, Q., Toews, M., Cosic, J., Jacques, J., Wiltshire, S., Lambert, J. et al. (2006) High-throughput affinity ranking of antibodies using surface plasmon resonance microarrays. Anal. Biochem. **351**, 241–253
30 Jostock, T., Vanhove, M., Brepoels, E., Van Gool, R., Daukandt, M., Wehnert, A., Van Hegelsom, R., Dransfield, D., Sexton, D., Devlin, M. et al. (2004) Rapid generation of functional human IgG antibodies derived from Fab-on-phage display libraries. J. Immunol. Methods **289**, 65–80
31 Beechem, J. M. (1992) Global analysis of biochemical and biophysical data. Methods Enzymol. **210**, 37–54
32 Kuzmic, P. (2006) A generalized numerical approach to rapid-equilibrium enzyme kinetics: application to 17β-HSD. Mol. Cell. Endocrinol. **248**, 172–181
33 Kuzmic, P. (1996) Program DYNAFIT for the analysis of enzyme kinetic data: application to HIV proteinase. Anal. Biochem. **237**, 260–273
34 Burnham, K. P., Anderson, D. R. and Burnham, K. P. (2002) Model selection and multimodel inference: a practical information–theoretic approach, Springer, New York
35 Bates, D. M. and Watts, D. G. (1988) Nonlinear regression analysis and its applications, Wiley, New York
36 Scuri, M., Botvinnikova, Y., Lauredo, I. T. and Abraham, W. M. (2002) Recombinant α_1-proteinase inhibitor blocks antigen- and mediator-induced airway responses in sheep. J. Appl. Physiol. **93**, 1900–1906
37 Raab, A. and Kemme, M. (2000) High-molecular-weight kininogen is a binding protein for tissue prokallikrein. FEBS Lett. **467**, 165–168
38 Christiansen, S. C., Zuraw, B. L., Proud, D. and Cochrane, C. G. (1989) Inhibition of human bronchial kallikrein in asthma. Am. Rev. Respir. Dis. **139**, 1125–1131
39 Forteza, R., Botvinnikova, Y., Ahmed, A., Cortes, A., Gundel, R. H., Wanner, A. and Abraham, W. M. (1996) The interaction of α_1-proteinase inhibitor and tissue kallikrein in controlling allergic ovine airway hyperresponsiveness. Am. J. Respir. Crit. Care Med.**154**, 36–42
40 Bizeto, L., Antunes, E., Portaro, F. C., Juliano, M. A., Juliano, L., Prado, E. S. and de Nucci, G. (1996) Pharmacological characterization of novel tissue kallikrein inhibitors *in vivo*. Immunopharmacology **32**, 111–114
41 Evans, D. M., Jones, D. M., Pitt, G. R., Ashworth, D., De Clerck, F., Verheyen, F. and Szelke, M. (1996) Synthetic inhibitors of human tissue kallikrein. Immunopharmacology **32**, 117–118

42 Griesbacher, T., Rainer, I., Tiran, B. and Evans, D. M. (2002) Involvement of tissue kallikrein but not plasma kallikrein in the development of symptoms mediated by endogenous kinins in acute pancreatitis in rats. Br. J. Pharmacol. **137**, 692–700
43 Wolf, W. C., Evans, D. M., Chao, L. and Chao, J. (2001) A synthetic tissue kallikrein inhibitor suppresses cancer cell invasiveness. Am. J. Pathol. **159**, 1797–1805
44 Szelke, M., Evans, D. M., Jones, D. M., Fawcett, L., Ashworth, D., Olsson, H., Featherstone, R. L. and Church, M. K. (1994) Synthetic inhibitors of tissue kallikrein: effects *in vivo* in a model of allergic inflammation. Braz. J. Med. Biol. Res. **27**, 1943–1947
45 Ellis, K. M. and Fozard, J. R. (2002) Species differences in bradykinin receptor-mediated responses of the airways. Auton. Autacoid Pharmacol. **22**, 3–16
46 Kirschvink, N. and Reinhold, P. (2008) Use of alternative animals as asthma models. Curr. Drug Targets **9**, 470–484
47 Abraham, W. M. (2008) Modeling of asthma, COPD and cystic fibrosis in sheep. Pulm. Pharmacol. Ther. **21**, 743–754
48 Watt, A. P., Schock, B. C. and Ennis, M. (2005) Neutrophils and eosinophils: clinical implications of their appearance, presence and disappearance in asthma and COPD. Curr. Drug Targets Inflamm. Allergy **4**, 415–423
49 Thie, H., Meyer, T., Schirrmann, T., Hust, M. and Dubel, S. (2008) Phage display derived therapeutic antibodies. Curr. Pharm. Biotechnol. **9**, 439–446
50 Deniz, Y. M. and Gupta, N. (2005) Safety and tolerability of omalizumab (Xolair), a recombinant humanized monoclonal anti-IgE antibody. Clin. Rev. Allergy Immunol. **29**, 31–48

Received 6 January 2009/9 June 2009; accepted 16 June 2009
Published as BJ Immediate Publication 16 June 2009, doi:10.1042/BJ20090010

Biochem. J. (2009) **422**, 383–392 (Printed in Great Britain) doi:10.1042/BJ20090010

online data

SUPPLEMENTARY ONLINE DATA

Specific inhibition of tissue kallikrein 1 with a human monoclonal antibody reveals a potential role in airway diseases

Daniel J. SEXTON*[1], Ting CHEN*, Diana MARTIK*, Petr KUZMIC†, Guannan KUANG*, Jie CHEN*, Andrew E. NIXON*, Bruce L. ZURAW‡, Rosanna M. FORTEZA§, William M. ABRAHAM¶ and Clive R. WOOD*

*Discovery Research, Dyax Corp., 300 Technology Square, Cambridge, MA 02139, U.S.A., †BioKin Ltd, 15 Main Street, Suite 232, Watertown, MA 02472, U.S.A., ‡Department of Medicine, University of California San Diego, 9500 Gilman Dr., La Jolla, CA 92093, U.S.A., §Division of Pulmonary and Critical Care Medicine, University of Miami, Miller School of Medicine, Miami, FL 33136, U.S.A., and ¶Department of Research, Mount Sinai Medical Center, 4300 Alton Road, Miami Beach, FL 33140, U.S.A.

INTRODUCTION

The purpose of this Supplementary Online Data is to summarize the details of the enzyme kinetic analysis that was used to determine (a) the molecular mechanism by which the human monoclonal antibody DX-2300 inhibits KLK1 and (b) the requisite kinetic constants. The raw experimental data consist of 72 reaction progress curves collected by using a 96-well plate reader. Inhibitor concentrations were varied from 0.087 nM to 5 nM (1.5-fold dilution ratio; 11 values; plus a control experiment at [I] = 0); substrate concentrations were varied from 26.3 μM to 200 μM (1.5-fold dilution ratio; six values).

DETERMINATION OF INITIAL RATES

In the first round of kinetic analysis we attempted to treat the reaction progress curves as perfect straight lines. The initial reaction rates were determined by simple linear regression; the initial rate generated by a linear fit is the slope of the regression line. The results of the linear regression of a representative progress curve are shown in the left-hand portion of Supplementary Figure S1. The initial reaction rate (slope of the regression straight line), v_0, is 5.75 fluorescence units/s.

The linear fit of the progress curve produces a systematic pattern in the distribution of residuals (bottom panel). Instead of the simple straight-line fit provided by the SoftMax software distributed with the plate reader (Molecular Devices), we used the software DynaFit [1] (BioKin) to generate a system of simultaneous differential equations and use those as a non-linear fitting model. The DynaFit software automatically generated the following system of simultaneous first-order ordinary differential equations, which then served as the regression model for the reaction progress:

$$\dot{c}_{\mathrm{E}} = -k_{\mathrm{aes}}c_{\mathrm{E}}c_{\mathrm{s}} + k_{\mathrm{des}}c_{\mathrm{E.S}} = k_{\mathrm{dep}}c_{\mathrm{E.S}} \quad (1)$$

$$\dot{c}_{\mathrm{S}} = -k_{\mathrm{aes}}c_{\mathrm{E}}c_{\mathrm{S}} + k_{\mathrm{des}}c_{\mathrm{E.S}} \quad (2)$$

$$\dot{c}_{\mathrm{E.S}} = -k_{\mathrm{aes}}c_{\mathrm{E}}c_{\mathrm{S}} + k_{\mathrm{des}}c_{\mathrm{E.S}} = k_{\mathrm{dep}}c_{\mathrm{E.S}} \quad (3)$$

$$\dot{c}_{\mathrm{P}} = +k_{\mathrm{dep}}c_{\mathrm{E.S}} \quad (4)$$

The c values are concentrations of the given species at an arbitrary time t. The 'dot' accent represents the first derivative with respect to time (e.g. $\dot{c}_{\mathrm{E}} = d[\mathrm{E}]/dt$).

The best-fit model represented by the system of eqns (1)–(4) is shown in the right-hand portion of Supplementary Figure S1. The distribution or residuals (bottom-right panel) is significantly more random than in the linear case. The initial rate computed from the non-linear model, v_0, is 6.22 fluorescence units/s, which is approx. 10 % higher than the initial rate obtained from the linear fit above ($v_0 = 5.75$ fluorescence units/s).

ANALYSIS OF INITIAL RATES

Model discrimination analysis: AIC_C

In the first round of model discrimination, we fitted the initial rates to four standard mechanistic models of enzyme inhibition (Supplementary Figure S2).

The corresponding portions of the DynaFit [1] input file are shown below.

```
[task]
   model = competitive ?
[mechanism]
   E + S <===> E.S          :     Ks    dissoc
   E.S ----> E + P          :     kcat
   E + I <===> E.I          :     Ki    dissoc
...
[task]
   model = uncompetitive ?
[mechanism]
   E + S <===> E.S          :     Ks    dissoc
   E.S ----> E + P          :     kcat
   E.S + I <===> E.S.I      :     Kis   dissoc
...
[task]
   model = noncompetitive ?
[mechanism]
   E + S <===> E.S          :     Ks    dissoc
   E.S ----> E + P          :     kcat
   E + I <===> E.I          :     Ki    dissoc
   E.S + I <===> E.S.I      :     Ki    dissoc
...
[task]
    model = mixed type ?
[mechanism]
   E + S <===> E.S          :     Ks    dissoc
   E.S ----> E + P          :     kcat
   E + I <===> E.I          :     Ki    dissoc
   E.S + I <===> E.S.I      :     Kis   dissoc
...
```

[1] To whom correspondence should be sent (email dsexton@dyax.com).

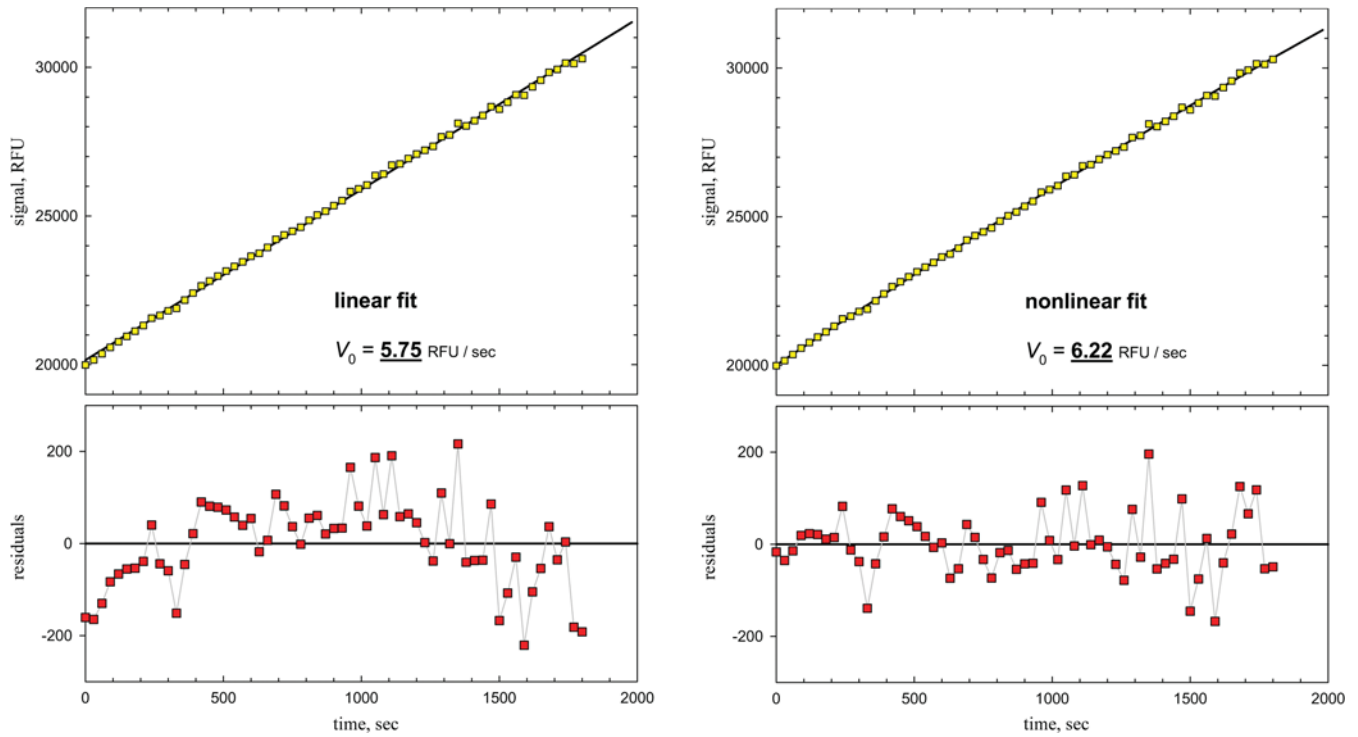

Figure S1 Linear fit of a representative progress curve (row C, column 2; [S] = 39.5 μM, [I] = 0) from *in vitro* assays of DX-2300 against KLK1 (left-hand panel) and a non-linear fit to a differential-equation model (right-hand panel)

Table S1 Initial rates in the inhibition of KLK1 with the monoclonal antibody DX2300

		Initial rate (v_0) (fluorescence units/s)					
[I] (nM)	[S] (μM) . . .	26.3	39.5	59.3	88.9	133.3	200.0
0		5.33	6.23	8.65	10.91	12.69	14.67
0.087		4.43	5.6	7.47	9.68	11.45	13.02
0.13		3.65	4.24	6.01	7.8	9.38	10.94
0.195		2.94	3.63	5.17	6.77	8.43	10.07
0.293		2.8	3.45	4.89	6.75	8.36	10.34
0.439		1.82	2.26	3.18	4.5	5.64	7.3
0.658		1.45	1.89	2.44	3.88	4.71	6.33
0.988		1.23	1.62	2.06	3.28	3.74	5.28
1.482		0.71	0.93	1.26	2.05	2.47	3.54
2.222		0.55	0.66	0.92	1.6	2.01	2.83
3.333		0.38	0.51	0.71	1.24	1.54	2.23
5		0.21	0.32	0.43	0.77	0.98	1.43

Table S2 *AIC*$_c$ for four standard models of enzyme inhibition

The number of data points (initial rates) is n_D for all candidate models

Model	n_P	SS_{rel}	AIC_c	ΔAIC_c	w
Competitive	4	1.065	177.6	2.2	0.253
Uncompetitive	4	4.322	278.4	103	0
Non-competitive	4	1.567	205.3	29.9	0
Mixed type	5	1	175.4	0	0.747

Table S3 Results of fitting to a mixed-type inhibition mechanism

Notes: [a]best-fit value; [b]formal standard error; [c]coefficient of variation; [d]lower limit of 95 % confidence interval; [e]upper limit of 95 % confidence interval.

Parameter	Fit[a]	StErr[b]	CV (%)[c]	Low$_{95\ \%}$[d]	High$_{95\ \%}$[e]
K_s (M)	76.3	6.7	8.8	60.5	96.4
k_{cat} (s^{-1})	33.8	29.6	87.7	10.9	>10 000
K_i (nM)	0.172	0.024	13.9	0.119	0.251
K_{is} (nM)	1.536	0.681	44.3	0.697	>53
[E] (nM)	0.060	0.0052	87.4	<0.0001	0.194

Table S4 Results of fitting to a competitive inhibition mechanism

Notes: [a]best-fit value; [b]formal standard error; [c]coefficient of variation; [d]lower limit of 95 % confidence interval; [e]upper limit of 95 % confidence interval.

Parameter	Fit[a]	StErr[b]	CV,%[c]	Low$_{95\ \%}$[d]	High$_{95\ \%}$[e]
K_s(M)	71.0	5.9	8.3	57.1	87.7
k_{cat} (s^{-1})	17.2	6.8	39.5	8.5	> 1000
K_i (nM)	0.132	0.009	6.6	0.111	0.157
[E] (nM)	0.113	0.045	40.1	< 0.001	0.232

The raw experimental data are summarized in Supplementary Table S1.

The DynaFit [1] software automatically generated a numerical fitting model as a system of simultaneous non-linear algebraic equations corresponding to each postulated mechanism. For example, the non-linear algebraic system corresponding to the competitive mechanism above is represented by the system of simultaneous non-linear algebraic eqns (5)–(8):

$$\tilde{c}_E = c_E + \frac{c_E c_S}{k_S} \quad (5)$$

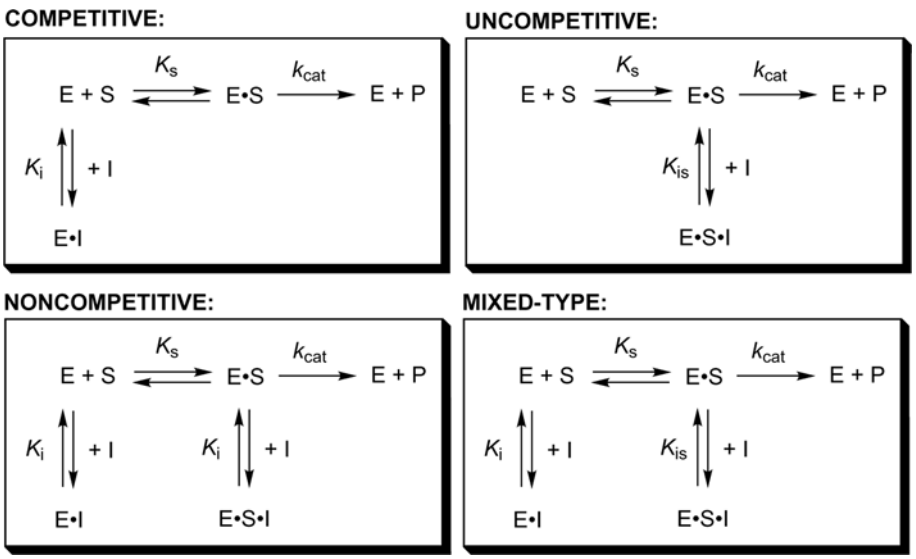

Figure S2 **Four standard mechanisms of enzyme inhibition examined in the first round of model-discrimination analysis**

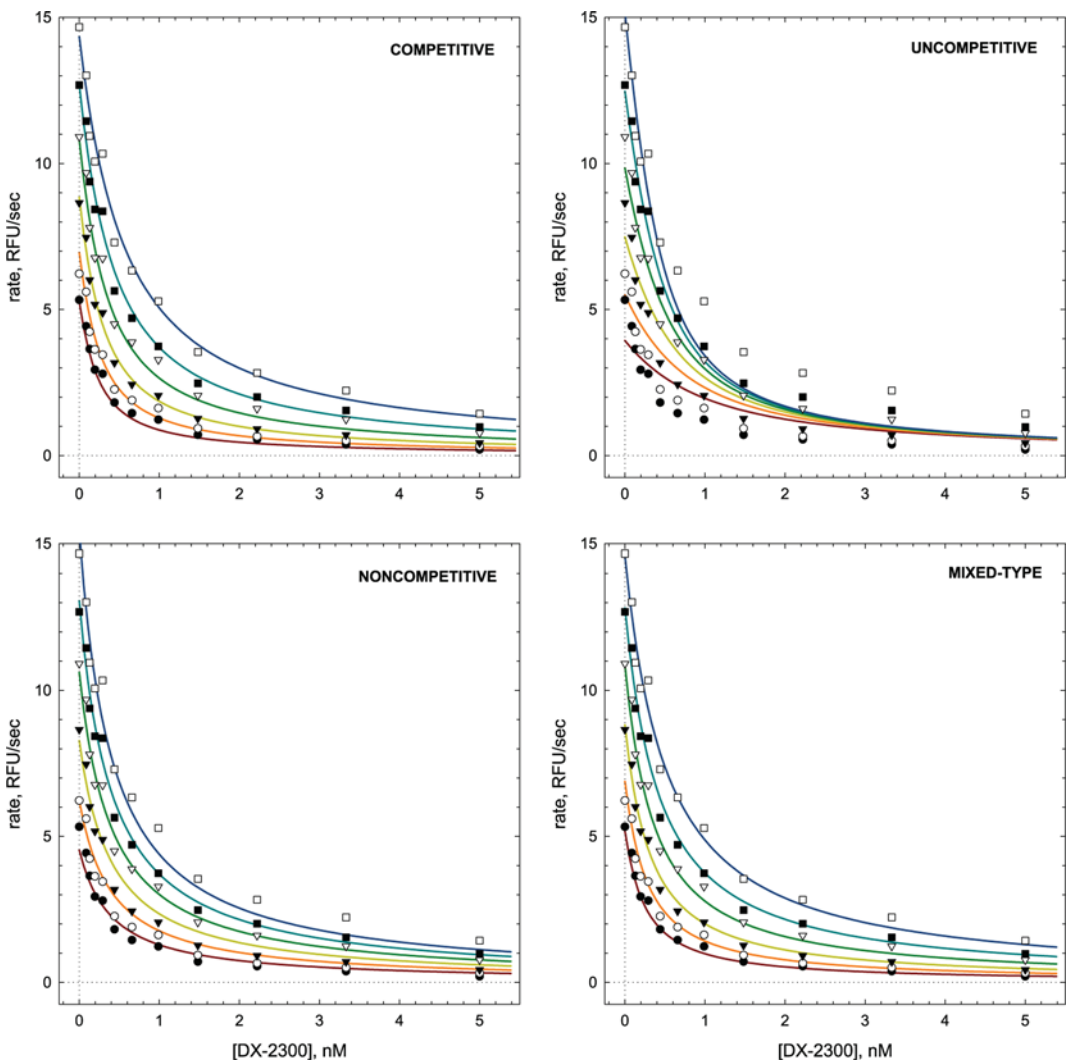

Figure S3 **Results of fitting to the four standard mechanisms of enzyme inhibition**

$$\tilde{c}_S = c_S + \frac{c_E c_S}{K_S} \quad (6)$$

$$\tilde{c}_I = c_I + \frac{c_E c_I}{K_i} \quad (7)$$

$$\tilde{c}_P = c_P \quad (8)$$

where the 'tilde' accent (~) represents the total or analytical concentration of each component species. The remaining c values are concentrations at equilibrium. This system of four non-linear algebraic equations for four uknowns (c_E, c_S, c_I and c_P) is solved numerically by the multi-dimensional Newton–Raphson method. This general numerical formalism accounts for the possibility of 'tight binding' [2–4]. The details of the algorithm are explained elsewhere [5].

The results of fitting to the four standard models of enzyme inhibition are summarized graphically in Supplementary Figure S3. The uncompetitive mechanism can be clearly excluded. The non-competitive mechanism also shows plainly visible deviations between the experimental data and the best-fit model. By contrast, the competitive and non-competitive mechanisms seem to fit the available data approximately equally well. This first impression is supported by rigorous statistical analysis, based on the second-order AIC_c [6,7].

Each of the four standard kinetic models was associated with a particular value of the final residual sum of squares and the corresponding AIC_c value. The results are summarized in Supplementary Table S2, where n_P is the number of adjustable model parameters, SS_{rel} is the residual sum of squares corresponding to each model, relative to the lowest value, AIC_c is the second-order AIC, ΔAIC_c is the differential AIC relative to the lowest value, and w is the Akaike weight [6]. The Akaike weight, w, measures the statistical probability, on a scale from zero to 1, that the given model is the 'true' model.

The results, summarized in Supplementary Table S2, show that the mixed-type non-competitive mechanism is associated with the lowest residual sum of squares ($SS_{rel} = 0$). However, this fact is relatively unimportant, because the mixed-type model contains a greater number of adjustable model parameters ($n_P = 5$) than the remaining models ($n_P = 4$). It is well known that any fitting model associated with a larger number of adjustable parameters (in this case, kinetic constants) has a tendency to produce a lower value of the residual sum of squares compared with a related model containing a smaller number of adjustable parameters. This tendency has nothing to do with which of the two candidate models (mechanisms) is more likely to be the 'true' model.

A much more important statistical measure for model discrimination is the AIC_c criterion or the associated Akaike weight, w. We can see in Supplementary Table S2 that the mixed-type model also is nominally the most favoured candidate among the four standard models being compared ($w = 0.75$). However, the competitive mechanism is closely behind, with $w = 0.25$, and the ΔAIC_c for the competitive model is only 2.2. According to Burnham and Anderson's heuristic rules [6], it is very hard, if not impossible, to discriminate between models that differ by less than ΔAIC_c. From the relatively low value of ΔAIC_c for the competitive model, we must conclude that, in this round of model-discrimination analysis, we were unable to differentiate between the competitive mechanism and the mixed-type mechanism. Both of these mechanisms appear approximately equally plausible. Only the uncompetitive mechanism ($\Delta AIC_c = 0$, $w = 0$) and the pure non-competitive mechanism ($\Delta AIC_c = 30$, $w = 0$) can be conclusively excluded from further consideration.

Confidence-interval estimation

The results summarized in Supplementary Table S2 mean that, solely on the basis of the values of AIC_c, it is not possible to discriminate between the competitive and mixed-type non-competitive models. Both mechanisms appear approximately equally plausible, with the mixed-type mechanism being very slightly preferred. To resolve this ambiguity, we performed confidence-interval estimation for the kinetic constants appearing in both mechanisms.

In Supplementary Figure S2 we can see that both models (competitive and mixed-type) share the inhibition constant, K_i. In addition, the mixed-type model contains the inhibition constant K_{is}. The question arises: 'what is the maximum plausible value of K_{is} within the given confidence level?'. If, hypothetically, we find that K_{is} could attain extremely high values (at the given probability level), this would mean that the ternary complex E·S·I is not formed (note that K_{is} is a dissociation equilibrium constant). In that case, the mixed-type mechanism reduces to the competitive mechanism.

The confidence intervals for parameters appearing in non-linear models are by definition non-symmetrical. Therefore we must use a suitable search method to establish the limits of the confidence interval. Here we use the profile-t method of Bates and Watts [8,9]. The essence of the profile-t confidence-interval search method, and an example of the determination of confidence interval for K_{is}, follow:

- A non-linear least-squares fit is performed with all model parameters appearing in the given model (in this case, we will optimize both K_i and K_{is} appearing in the mixed-type model)
- In a sequence of follow-up least-squares regressions, we 'step' with K_{is} progressively away from its optimal value in either direction (first toward higher then optimal values, and then towards lower than optimal values)
- At each step, we hold the K_{is} value fixed, but optimize all the remaining model parameters (in this case, K_i, K_s and K_{cat})
- At each step (at the given fixed value of K_{is}), we compare the resulting locally optimal value of the sum-of-squares (*SSQ)* with the globally optimal value. Inevitably, the locally optimal *SSQ* value will be somewhat higher than the globally optimal *SSQ* value – because, in each additional least-squares regression analysis, we are holding K_{is} fixed at a worse-than-optimal value.
- As soon as the locally optimal *SSQ* value reaches a particular critical value, SSQ_{crit}, we record the corresponding value of K_{is}. This is the limit (upper or lower) of its confidence interval.

The critical value SSQ_{crit} is related to the globally optimal value SSQ_{min} through the critical value of the Fisher's F-statistic at the given probability level. For details, see [8,9].

In certain special cases, stepping with the given model parameter away from its optimal value (while optimizing all the remaining model parameters) might increase the local *SSQ* only very slightly, no matter how large a step we take. Even very large changes in the given model parameter will produce increases in the local *SSQ* that are lower than the critical value SSQ_{crit}. In these special cases, we say that the given confidence interval is open-ended, meaning that the given model parameter could plausibly attain an infinitely large value.

The results of the profile-t confidence-interval search for K_i and K_{is} are summarized in Supplementary Table S3 and illustrated graphically in Supplementary Figure S4. Closed-circle symbols in Supplementary Figure 4 represent the best-fit values of both inhibition constants ($K_i = 0.17 \pm 0.02$ nM; $K_{is} = 1.5 \pm 0.6$ nM); corresponding to these values is the globally minimal sum of squares, SSQ_{min}. Open-triangle symbols represent the locally

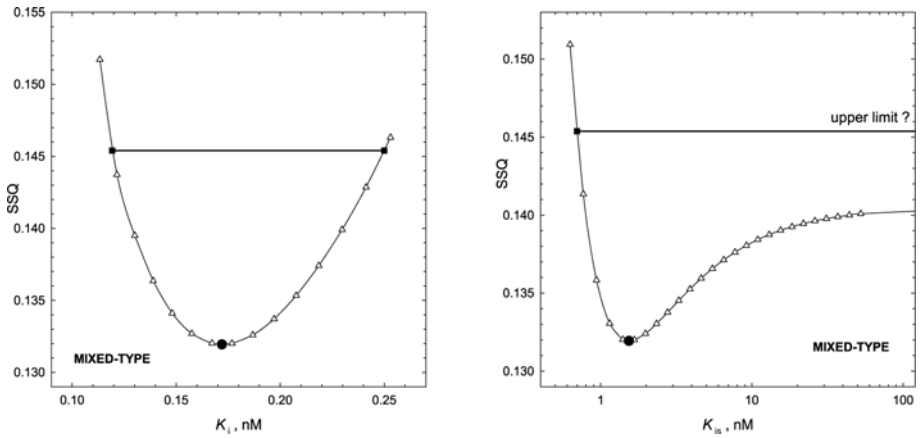

Figure S4 Confidence-interval estimation for K_i and K_{is} appearing in the mixed-type mechanism (99 % probability level)

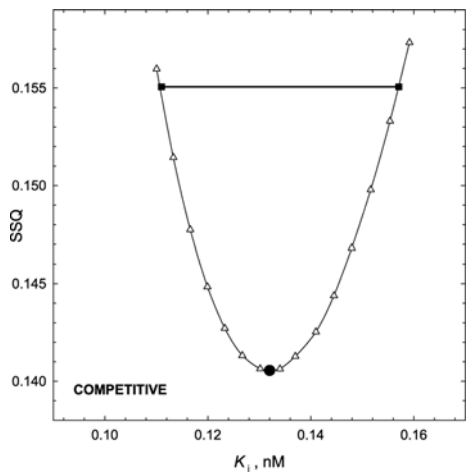

Figure S5 Confidence-interval estimation for K_i appearing in the competitive mechanism (99 % probability level)

minimal values of *SSQ* at various fixed values of the given inhibition constant, while all the remaining model parameters are optimized. The thick horizontal line corresponds the critical value of the sum-of-squares, SSQ_{crit}. Closed-square symbols represent the confidence interval limits for K_i (left panel) and K_{is} (right panel). The limits are found where the horizontal line drawn at SSQ_{crit} intersects with the hyper-surface of the locally optimized sum-of-squares in the parameter space [9].

Supplementary Figure S4 shows that the 99 % confidence-level interval for the inhibition constant K_i (appearing in the mixed-type mechanism) is well defined. The lower limit of the confidence interval is at $K_i = 0.11$ nM and the upper limit is at $K_i = 0.25$ nM. Note that the confidence interval is (a) slightly non-symmetrical and (b) significantly wider than is suggested the formal standard error (± 0.02 nM).

By contrast, the confidence interval for K_{is} is open-ended. Only the lower limit could be reliably determined at $K_{is} = 0.70$ nM. However, while searching for the upper end of the confidence interval, the profile-t method [8,9] terminated at $K_{is} = 53$ nM without a sufficient increase in the *SSQ* value; the critical value SSQ_{crit} could not be reached, regardless of how low K_{is} is. This means that, at the 99 % confidence level, the inhibition constant K_{is} might reach an infinitely high value without the goodness-of-fit deteriorating significantly.

Importantly, if the dissociation constant K_{is} can plausibly reach infinitely large values, the mixed-type non-competitive mechanism actually reduces to the competitive mechanism, because K_{is} means that the E · S · I complex essentially is not formed at all. Thus we conclude that DX-2300 is a competitive inhibitor of KLK1.

The confidence interval for K_i appearing in the competitive mechanism is shown in Supplementary Figure S5 (see also Supplementary Table S4). At the 99 % probability level, the interval ranges from $K_i = 0.11$ nM to $K_i = 0.16$ nM, with the best-fit value approximately $K_i = 0.13$ nM. As before, note that the confidence interval is slightly non-symmetrical, as it must be, in principle, because the fitting model is non-linear.

It is worth noting the best-fit values and the associated non-symmetrical confidence intervals for the enzyme concentration, [E], which is treated as an adjustable model parameter. In Supplementary Table S4, as well as in Supplementary Table S3, we see that the actual enzyme concentration in the assay must be significantly lower than the nominal concentration ($[E]_{nom} = 0.5$ nM). Within the competitive mechanism, the best-fit value is $[E]_{fit} = 0.11$ nM, which corresponds to approx. 22 % activity.

The enzyme concentration is quite poorly defined by these data, which is reflected in the fact that the lower limit of the 99 % confidence interval for [E] could not be established. At the 99 % confidence level, the plausible values of [E] asymptotically tend to zero. To put this into plain language, on the basis of this particular data set, we simply cannot tell just how low [E] could be.

On the other hand, we can quite clearly see the upper limit of the 99 % confidence-level interval ($[E]_{Up} = 0.23$ nM). In plain language, we can be quite certain that the enzyme concentration is not higher than 0.23 nM. At the nominal concentration ($[E]_{nom} = 0.5$ nM), this corresponds to at most 50 % of the total enzyme being catalytically active.

Incidentally, the upper limit for k_{cat} in Supplementary Tables S3 and S4 could not be established either, because k_{cat} and [E] are statistically 'coupled' or correlated in the non-linear fitting models. In other words, the same set of data could be equally

well described by many different combinations (pairs) of k_{cat} and [E] values – as long as these values in each pair are inversely proportional to each other.

SUMMARY AND CONCLUSIONS

We established the following basic properties of DX-2300:

- The antibody DX-2300 is a competitive inhibitor of KLK1
- The inhibition constant, K_i, is 0.13 nM (99 % confidence interval from 0.11 nM to 0.16 nM)

With regard to the proper method of data analysis, we observed that even slight non-linearities seen in the kallikrein progress curves (<2 % of the total signal range) translate into significant distortions of the initial rates (>15 % systematic error). This calls for non-linear fitting of progress curves using the appropriate (preferably mechanistic) model.

Received 6 January 2009/9 June 2009; accepted 16 June 2009
Published as BJ Immediate Publication 16 June 2009, doi:10.1042/BJ20090010

REFERENCES

1 Kuzmič, P. (1996) Program DYNAFIT for the analysis of enzyme kinetic data: application to HIV proteinase. Anal. Biochem. **237**, 260–273
2 Morrison, J. F. (1969) Kinetics of the reversible inhibition of enzyme-catalysed reactions by tight-binding inhibitors. Biochim. Biophys. Acta **185**, 269–286
3 Cha, S. (1975) Tight-binding inhibitors. I. Kinetic behavior. Biochem. Pharmacol. **24**, 2177–2185
4 Williams, J. W. and Morrison, J. F. (1979) The kinetics of reversible tight-binding inhibition. Methods Enzymol. **63**, 437–467
5 Kuzmič, P. (2006) A generalized numerical approach to rapid-equilibrium enzyme kinetics: Application to 17 β-HSD. Mol. Cell. Endocrinol. **248**, 172–181
6 Burnham, K. B. and Anderson, D. R. (2002) Model Selection and Multimodel Inference: A Practical Information-Theoretic Approach, 2nd edn., Springer-Verlag, New York
7 Myung, J. I. and Pitt, M. A. (2004) Model comparison methods. Methods Enzymol. **383**, 351–366
8 Brooks, I., Watts, D., Soneson, K. and Hensley, P. (1994) Determining confidence intervals for parameters derived from analysis of equilibrium analytical ultracentrifugation data. Methods Enzymol. **240**, 459–478
9 Bates, D. M. and Watts, D. G. (1988) Nonlinear Regression Analysis and its Applications, Wiley, New York